

AD-A100 599

WISCONSIN UNIV-MADISON MATHEMATICS RESEARCH CENTER
TRAPPING OF WATER WAVES ABOVE A ROUND SILL. (U)

F/G 20/4

MAR 81 Y YAMAMURO

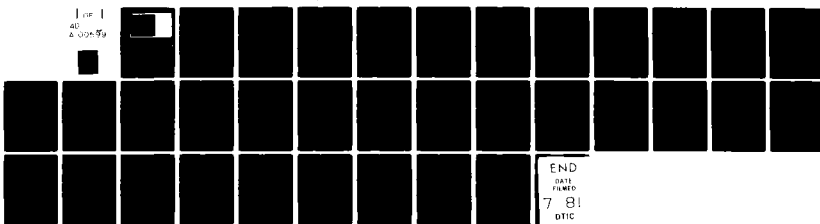
DAAG29-80-C-0041

UNCLASSIFIED

MRC-TSR-2195

NL

Line 1
40
4-000598



END
DATE
FILED
7-81
DTIC

14
100-781-2195
2
AD A100599

MRC Technical Summary Report # 2195

TRAPPING OF WATER WAVES
ABOVE A ROUND SILL.

Yuriko Yamamuro

Mathematics Research Center
University of Wisconsin-Madison
610 Walnut Street
Madison, Wisconsin 53706

FTIC
JUN 25 1981

11 Mar 81

(Received February 9, 1981)

FILE COPY

Sponsored by

U. S. Army Research Office
P. O. Box 12211
Research Triangle Park
North Carolina 27709

Approved for public release
Distribution unlimited

and

National Science Foundation
Washington, D.C. 20550

(2)

UNIVERSITY OF WISCONSIN - MADISON
MATHEMATICS RESEARCH CENTER

TRAPPING OF WATER WAVES ABOVE A ROUND SILL

Yuriko Yamamuro

Technical Summary Report #2195

March 1981

ABSTRACT

The three-dimensional problem of wave-trapping above a submerged round sill was first analyzed by Longuet-Higgins (1967) on the basis of a linear shallow-water theory. The large responses predicted by the theory were, however, not well borne out by the experiments of Barnard, Pritchard and Provis (1981) and this has motivated a more detailed study of the problem. A full, linear theory for both inviscid and weakly viscous fluid, without any shallow-water assumptions, is presented here. It reveals important limitations on the use of shallow-water theory and the reasons for them. In particular, while the qualitative features of wave-trapping are similar to those of shallow-water theory, the nearly-resonant frequencies differ significantly, and since the resonances are narrow, the observed amplitudes at a given frequency differ greatly. The geometry is strongly indicative of long waves and the dispersion relation appears quite consistent with that, but the part of the motion at wave numbers that are not small has, despite the small amplitude, a substantial effect on the response to excitation.

AMS (MOS) Subject Classification: 76B15

Key Words: surface gravity water waves, diffraction, trapping modes.

Work Unit Number 2 - Physical Mathematics

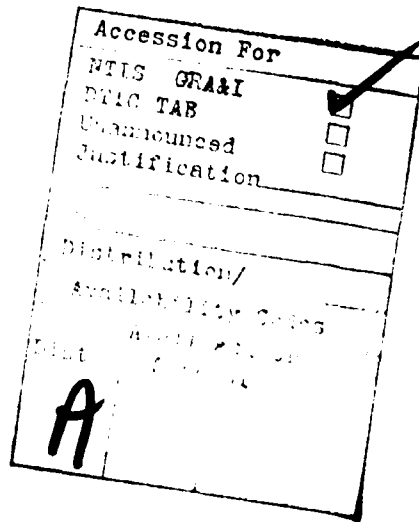
DISTRIBUTION STATEMENT A

Approved for public release;
Distribution Unlimited

Sponsored by the United States Army under Contract No. DAAG29-80-C-0041. This material is based upon work supported by the National Science Foundation under Grant No. MCS-7927062.

SIGNIFICANCE AND EXPLANATION

Observations of wave records at Macquarie Island, in the ocean south of Australia, have shown augmented response at certain frequencies. It has been established that these observations can be explained as due to the resonant excitation, of trapped modes, by the surrounding wave field. This phenomenon has prompted considerable interest in the possibility of wave trapping. Theories, based on the approximation of shallow water, lead to predictions of very sharp resonances but these have not been observed in the laboratory. This paper develops a full linear theory, including damping, for a special geometry, and thus serves to define the limitations in the results obtained by using shallow-water theory.



The responsibility for the wording and views expressed in this descriptive summary lies with MRC, and not with the author of this report.

TRAPPING OF WATER WAVES ABOVE A ROUND SILL

Yuriko Yamamoto

§1. Introduction

A theoretical study of the trapping that results when a train of small-amplitude, plane waves of a fixed frequency is incident on a submerged, steep-sided, round sill (Figure 1) was made by Lonquet-Higgins (henceforth referred to as LH) in 1967. His investigation was motivated by wave records taken at Macquarie Island showing the occurrence of regular oscillations of unusually large amplitudes. In view of these observations, LH considered a simplified geometry in which the island shelf was represented by a round sill, with a circumference of 80 km, submerged to a depth of 100 m. He based his calculation on linear, inviscid, shallow-water theory and used separation of variables in cylindrical coordinates to determine the expressions for the surface displacements for each of the two regions of constant depths. Because of the depth-independence of the velocity field in shallow-water theory, the velocity components could not be made continuous at the sill edge, and two approximate matching conditions were used: the continuity of surface elevation and the continuity of the horizontal component of the mass flux. LH's (1967) analysis showed the existence of eigenfrequencies with very small imaginary parts. A train of plane waves with a frequency near such an eigenfrequency could theoretically excite "nearly-trapped" modes over the sill, and the response at such modes was determined. The largest responses were found to occur at the higher angular modes and at smaller ratios of the

Sponsored by the United States Army under Contract No. DAAG29-80-C-0041. This material is based upon work supported by the National Science Foundation under Grant No. MCS-7927062.

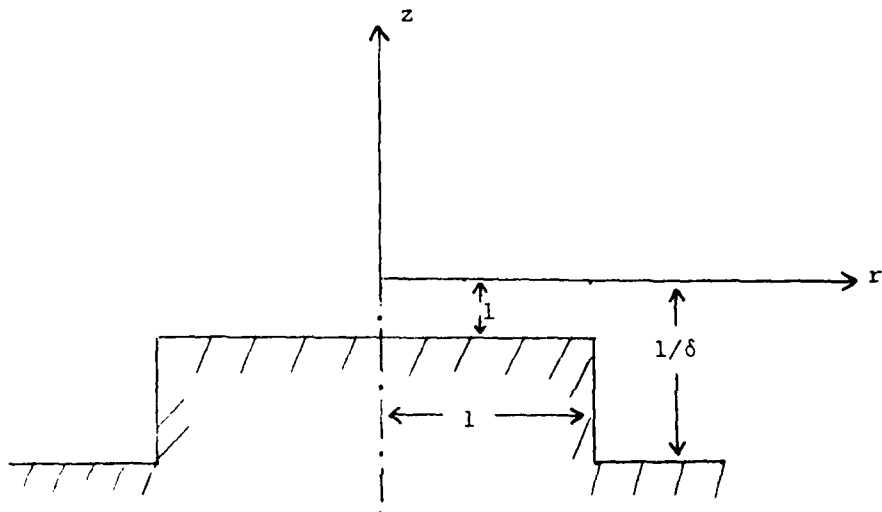


Figure 1

depths. These calculations have been confirmed and extended by Summerfield (1969), who applied shallow-water theory to a "shelf-island" model consisting of a steep sided round island rising from the top of a round sill of larger radius. He showed the eigenfrequencies for his system to be closely related to those of LH's sill geometry. However, laboratory observations by Pite (1977) and by Barnard, Pritchard and Provis (1981) (henceforth denoted by BPP) did not reveal the large responses predicted by the shallow-water model. The purpose of this paper is to examine a complete linear theory in an endeavor to explain these discrepancies.

In §2, the equations governing the full linear inviscid theory are presented. In §3, the velocity potential is calculated. This is achieved by representing it separately in the regions above the sill and outside the sill; the solutions in the two zones are then made to satisfy the necessary conditions of analytic continuation at the sill-edge. This leads to an

infinite set of linear equations, for which a collocation method of solution is described. In addition, an iterative method is presented as a check on the extensive calculations.

In §4, the theory is applied to laboratory conditions relating to the experiments of BPP. The results show that the modes that decay away from the sill-edge and are not included in shallow-water theory, make appreciable contributions to the wave amplitudes above the sill. To obtain a comparison on oceanographic scales between the full theory and the shallow-water theory, the theoretical predictions for the special case of LH's sill geometry are examined in §5. The differences are particularly striking near the frequencies where the full theory predicts large amplitudes, and the reasons for these differences are discussed. A theory allowing for weakly viscous effects is given in §6. Numerical computations were carried out at a frequency pertaining to the conditions considered by BPP. At that frequency, viscous effects were found to have negligible influence on the amplitudes. For the entire range of frequencies investigated by BPP, moreover, viscous effects are estimated to make less than 1% difference in the amplitudes, even at the frequencies where peak amplitudes are predicted. On oceanographic scales, however, where an eddy viscosity may be more appropriate than the kinematic viscosity, damping may be more pronounced.

§2. General equations

The motion is assumed inviscid, simple-harmonic in time, and of sufficiently small amplitude for the use of linear theory. It is referred to cylindrical coordinates r, θ, z with the origin at the undisturbed water surface (see Figure 1), r measured outward in units of the sill radius a , and z measured vertically upward in units of the undisturbed water depth d above the sill; the depth outside the sill is denoted by $D = d/\delta$. Let x denote the horizontal coordinate in the direction $\theta = 0$. A train of plane waves, of frequency σ and amplitude $|n^*|_I$, is incident on the sill from the positive x -axis. The surface displacement, measured in units of d , is denoted by n and the velocity potential $\phi(r, \theta, z, t)$ is measured in units of $d^2\sigma$ and satisfies Laplace's equation namely

$$\frac{\partial^2 \phi}{\partial r^2} + \frac{1}{r} \frac{\partial \phi}{\partial r} + \frac{1}{r^2} \frac{\partial^2 \phi}{\partial \theta^2} + \frac{a^2}{d^2} \frac{\partial^2 \phi}{\partial z^2} = 0 \quad , \quad (2.1)$$

together with the following boundary conditions: at the free surface, $z = 0$,

$$n_t = \sigma \phi_z$$

and $\phi_{tt} + q/d \phi_z = 0, r > 0, 0 < \theta < 2\pi ; \quad (2.2a)$

on the horizontal portion of the seabed, $z = -1$ and $0 < r < 1$, and $z = -1/\delta, r > 1$,

$$\phi_z = 0 ; \quad (2.2b)$$

and on the vertical wall of the sill at $r = 1$, $-1/\delta < z < 1$,

$$\phi_r = 0 . \quad (2.2c)$$

At large distances from the sill, the wave-field is assumed to consist of the incident wave, whose surface elevation is the real part of

$$\eta_I = |\eta|_I e^{-i(Kx+\sigma t)}$$

together with waves that either decay or radiate outwards. Here, K is the positive real root of the dispersion relation

$$(KD/a) \tanh (KD/a) = D\sigma^2/g . \quad (2.3)$$

Different representations of the solution will be used in the domain above the sill, $r < 1$, and in that outside the sill, $r > 1$. These functions must be analytic continuations of each other, for which a necessary and sufficient condition is the continuity of ϕ and $\partial\phi/\partial r$.

§3. Form of solutions

Let the velocity potentials for $r < 1$ and $r > 1$ be denoted by ϕ_s and ϕ_0 respectively, and be simple harmonic in time with radian frequency σ . Make the decomposition $\phi_0 = \phi_I + \phi_R$ where ϕ_I represents the incident plane wave train and ϕ_R represents waves generated by the sill. ϕ_I is calculated by separation of variables in Cartesian coordinates:

$$\phi_I = \frac{1}{2} |\eta|_I e^{-i(a\lambda_0 x/D + \sigma t)} \frac{\cosh \lambda_0(\delta z + 1)}{\lambda_0 \sinh \lambda_0} + * . \quad (3.1)$$

Here, and throughout the paper, the notation $+ *$ will be used to denote the addition of the complex conjugate of all preceding terms. The free-surface boundary conditions require λ_0 to be the real and positive root of the dispersion relation (e.g. see Davis & Hood 1976)

$$\lambda \tanh \lambda = D\sigma^2/q . \quad (3.2)$$

For convenience, the expression for ϕ_I is converted to cylindrical coordinates (Bateman Manuscript Project 1953, Vol. 2, §7.2.4, p. 7, Eqn. 27):

$$\phi_I = e^{-i\sigma t} \frac{\cosh \lambda_0(\delta z + 1)}{2\lambda_0 \sinh \lambda_0} \sum_{m=0}^{\infty} \epsilon_m^{-m} J_m(a\lambda_0 r/D) \cos m\theta + * , \quad (3.3)$$

where $\epsilon_m = \begin{cases} 1 & \text{if } m = 0 \\ 2 & \text{if } m \neq 0 \end{cases}$. For the purpose of computations for the linearized problem, $|\eta|_I$ is normalized to unity.

The generated field in the region outside the sill, $r > 1$, may be represented as the sum (Havelock 1929)

$$\begin{aligned}
\phi_R = & e^{-i\sigma t} \sum_{m=0}^{\infty} \cos m\theta \{ B_{m0} H_m^{(1)}(a\lambda_0 r/D) \cosh \lambda_0(\delta z+1) \\
& + \sum_{n=1}^{\infty} B_{mn} K_m(a\lambda_n r/D) \cos \lambda_n(\delta z+1) / K_m(a\lambda_n/D) \} + * .
\end{aligned} \tag{3.4}$$

Here, elements of $\{\pm i\lambda_m : m = 1, 2, \dots\}$ are the purely imaginary roots of the dispersion relation (3.2). Note that the model expansion is complete (Davis & Hood 1976) and that $\lambda_m = m\pi$ for m sufficiently large or for $D\sigma^2/q$ sufficiently small. The notations for the Bessel functions are those of Abramowitz and Stegun (1972, §9). Each term in (3.4) satisfies the appropriate conditions at infinity as well as the free-surface conditions and boundary conditions on the seabed. The, as yet undetermined, coefficients B_{m0} and B_{mn} ($n \neq 0$) are, respectively, coefficients of each radiating mode and each non-radiating mode, which is confined near the sill-edge. From now on, the subscript on λ_0 and the superscript on the Hankel function will be dropped.

The solution in the sill-region, $r < 1$, may be represented as the sum of solutions obtained by separation of variables, namely

$$\begin{aligned}
\phi_s = & e^{-i\sigma t} \sum_{m=0}^{\infty} \cos m\theta \{ A_{m0} J_m(akr/d) \cosh k(z+1) \\
& + \sum_{n=1}^{\infty} A_{mn} I_m(ak_n r/d) \cos k_n(z+1) / I_m(ak_n/d) \} + * .
\end{aligned} \tag{3.5}$$

Here, elements of $\{k_0, ik_n : n = 1, 2, \dots\}$ are the roots of

$$k \tanh k = d\sigma^2/q \tag{3.6}$$

of which each of the k_n are positive. Each term satisfies the appropriate conditions at the edge of the sill, at the free-surface and on the seabed.

The, as yet undetermined, coefficients A_{m0} and A_{mn} ($n \neq 0$) are, respectively, coefficients of each wavelike mode and each spatially decaying mode. In what follows, the subscript on k_0 will be dropped.

The continuity of $\partial\phi/\partial r$ at $r = 1$, $-1 < z < 0$, $0 < \theta < 2\pi$, yields one of the two conditions at the sill-edge:

$$\frac{\partial\phi_0}{\partial r} = \begin{cases} \frac{\partial\phi_s}{\partial r} & \text{for } -1 < z < 0 \\ 0 & \text{for } -1/\delta < z < -1 \end{cases} \quad (3.6)$$

By virtue of the orthogonality property of the set $\{\cosh \lambda(\delta z + 1), \cos \lambda_n(\delta z + 1) : n = 1, 2, \dots\}$, this condition yields, for $m = 0, 1, \dots$

$$[B_{m0} H'_m(a\lambda/D) + F_m^*] \frac{a\lambda}{D} h(\lambda) = \int_{-1}^0 \frac{\partial\phi_m}{\partial r} \Big|_{r=1} \cosh \lambda(\delta z + 1) dz. \quad (3.7)$$

Here ϕ_m denotes the coefficient of $\cos m\theta e^{-i\omega t}$ in ϕ_s and F_m^* and $h(\lambda)$ are defined in the appendix. For $n = 1, 2, \dots$,

$$B_{mn} \frac{K'_m(a\lambda_n/D)}{K_m(a\lambda_n/D)} \frac{a\lambda_n}{D} h(i\lambda_n) = \int_{-1}^0 \frac{\partial\phi_m}{\partial r} \Big|_{r=1} \cos \lambda_n(\delta z + 1) dz.$$

The second condition at $r = 1$, $-1 < z < 0$, $0 < \theta < 2\pi$, is the continuity of ϕ . This yields a second relation between B_{mn} and A_{mn} , from which the B_{mn} are eliminated by means of equations (3.7). The resulting equations for the A_{mn} are:

$$\begin{aligned} A_{m0} \{ \cosh k(z+1) J_m(ak/d) - \ell_{m0}(z) \} + \sum_{p=1}^{\infty} A_{mp} \{ \cos k_p(z+1) - \ell_{mp}(z) \} \\ = \{ F_m - F_m^* \frac{H_m(a\lambda/D)}{H'_m(a\lambda/D)} \} \cosh \lambda(\delta z + 1) \quad \text{for } -1 < z < 0, m = 0, 1, \dots \end{aligned} \quad (3.8)$$

The notation is defined in the appendix. When no spatially decaying modes are included, equation (3.8) is first multiplied by $\cosh k(z+1)$ and then integrated over z . With the inclusion of the decaying modes, a collocation method is used to solve the resulting infinite number of equations: that is, an N by N matrix equation is constructed by the application of equation (3.8) at N values of z in the range $-1 < z < 0$ and by neglecting the higher-order decaying modes $\{A_{mp} : p > N\}$.

Justification for the matrix truncation, which is performed in the calculations of the following sections, is as follows. For the investigation on the laboratory scales described in §4, the N values of z were chosen to be $\{z : z = -i/(N+1), i = 1, \dots, N\}$ for $N = 2, 6, 11, 16, 21, 41$. It is shown in §4 that the differences in the resulting amplitudes for $N > 6$ was of negligible importance. Hence, it is apparent that the above choice for the values of z , with $N = 6$, was adequate for computations involving similar sill geometries. The computations in §5 concern scales, for which the parameter a/d was much greater than in §4, so that the local modes decayed faster away from the sill-edge than those of §4. Since experimental results by Pite (1977) and, independently, by PTP indicated almost no presence of exponential decay in the wave-field near the sill-edge, it is expected that the faster the local modes decay, the less will be their response. Therefore, $N = 6$, which was sufficiently accurate for §4, was also expected to give suitable accuracy for §5, and has also been used for the computations described in §5.

The computations are made difficult by the presence, in equation (3.8), of the infinite series in the terms $\ell_{mp}(z)$ for $n = 0, 1, \dots, m = 0, 1, \dots$, which are slowly convergent. Because of this, a numerical check on the complicated computations was required, and an iterative method is now presented for this purpose.

The decomposition of ϕ_s in the radial variable yields (as shown by equation (3.5)) a principal part $J_m(akr/d)$, which is wavelike, and an infinite number of modes $I_m(ak_n r/d)$ that decay away from the sill-edge. If the value of the principal radial eigenfunction at the sill-edge is not too small, then an iterative procedure may be adopted. From now on, the coefficient of $\cos m\theta e^{-i\omega t}$ in ϕ_s and ϕ_0 will be denoted by ϕ_m .

A preliminary outer flow is determined from the radiation condition and the boundary condition $\partial\phi_m/\partial r = 0$ at $r = 1$, $-1 < z < 0$. This outer flow then determines the boundary condition at $r = 1$, $-1 < z < 0$, for a sill flow, through the continuity of ϕ . This sill flow then yields $\partial\phi_m/\partial r$ at $r = 1$, $-1 < z < 0$, from which a second outer flow is calculated, and so forth.

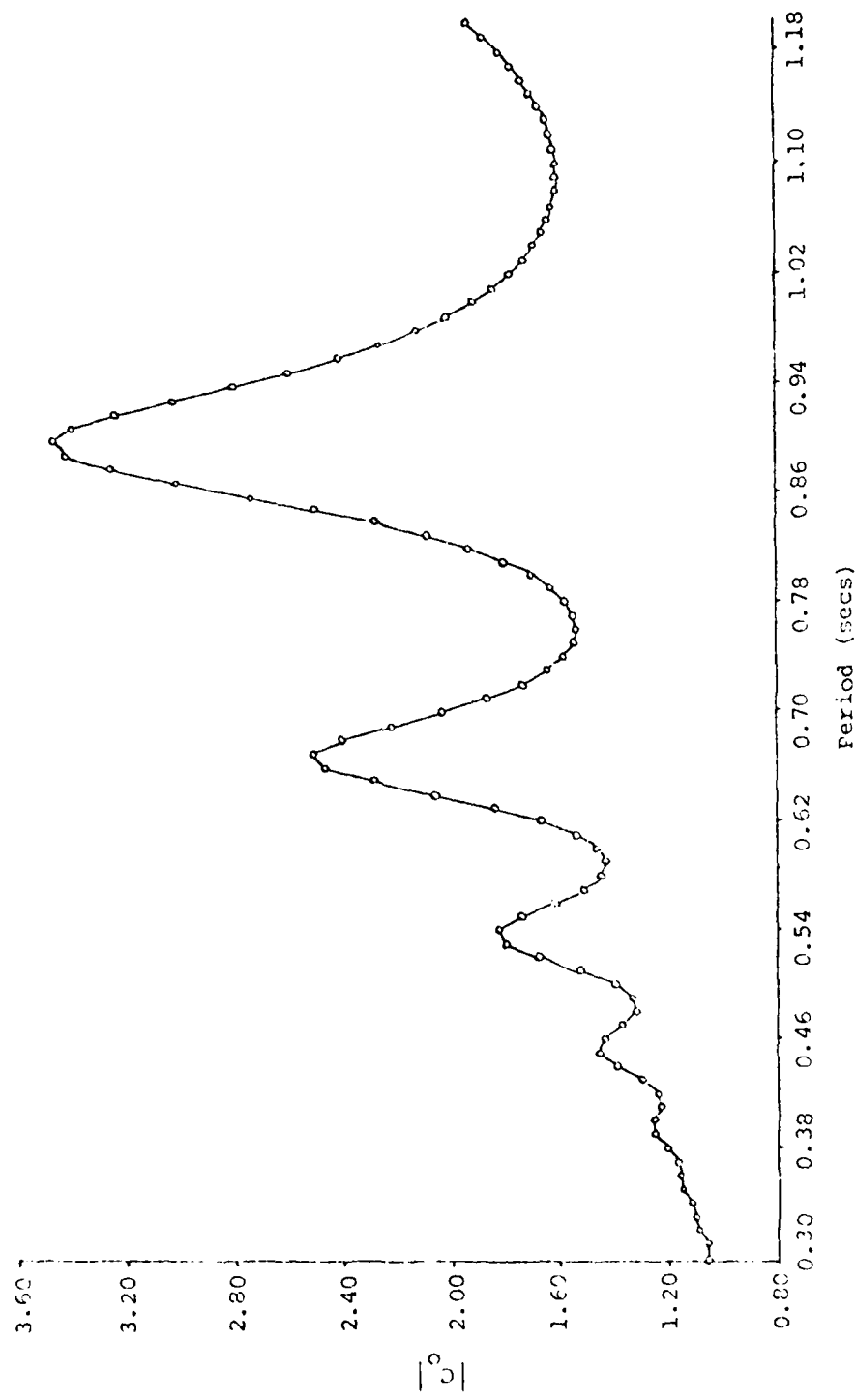
Equations (A) and (B) of the appendix arise from this scheme and are to be used as follows. When the A_{mn} in ϕ_s are known, the coefficient B_{mn} of ϕ_0 are calculated from the equations (A). Note that here, $H_m'(a\lambda/D)$, $I_m(ak_n/d)$ and $K_m'(a\lambda_p/D)$ do not vanish. When the B_{mn} are known, the coefficients in ϕ_s are calculated from the equations (B). This iteration diverges near the zeros of $J_m(ak/d)$, which lie near the peak periods. This scheme therefore fails for the parameters of most interest, but it was felt important to use the method to provide a check on the computations made with (3.8).

§4. Application to laboratory scales

This section concerns some calculations made to correspond to the laboratory scales used by BPP. For their experiments, $a = 50$ cm, $d = 1.75$ cm, $D = 15.4$ cm and the forcing periods ranged between 0.75 and 1.20 seconds.

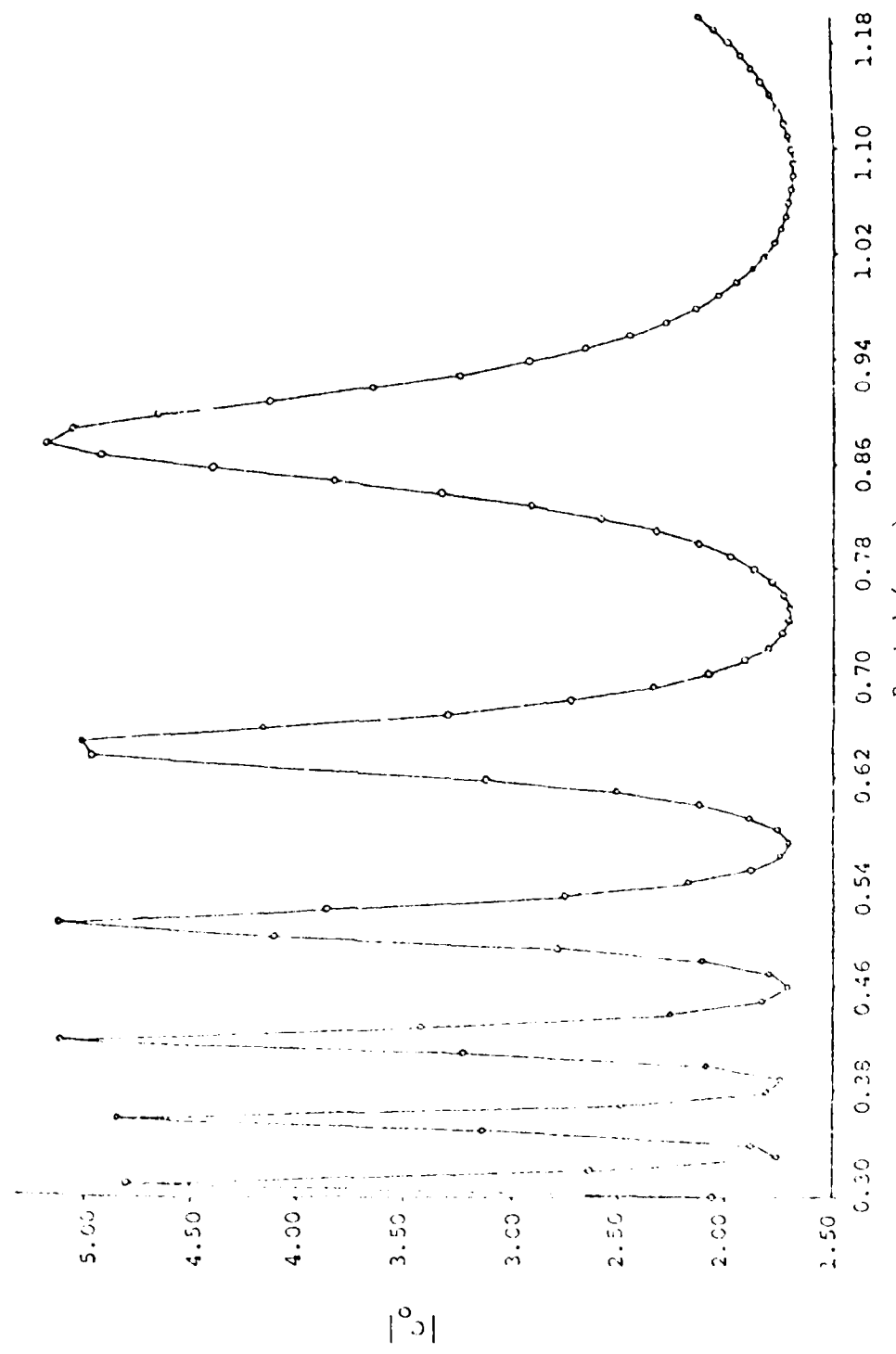
The full linear theory with no spatially decaying modes was used to compute the response curve for each model number and were compared with the linear shallow-water theory. Figures 4.1(a) and 4.1(b) display the results for the 0th mode and figure 4.2 those of the 6th mode. The curves show that the peaks in the lower frequency range occurred near those of linear shallow-water theory. At small modal numbers, however, the response was significantly diminished and at large modal numbers, the bandwidths were small so that the LH theory was not useful in calculations of the amplitudes. In the higher frequency range, there was no evidence of the peaked response predicted by the LH theory. In this connection, note that there are a large number of zeros in the radial eigenfunction $J_m(akr/d)$ in the sill-region. Thus, the horizontal scale of the motion is so much smaller than the radius that the motion is not a long wave, and this is the most probable source of the substantial error in that theory.

Computations, accounting also for the decaying modes, were carried out at the forcing period of 1.181 seconds where the measurements by BPP yielded the largest amplitude above the sill. The difference between the empirical values $(|\eta_E(r_i, \theta_i)| : r_i = 1/14 + (i-1)/7, i = 1, \dots, 7, \theta_i = (i-1)/18, i = 1, \dots, 19)$ and the theoretical values $(|\eta_T|)$ of the wave amplitudes was measured by



Linear theory response with no "decaying" modes, for the BPP sill, mode number is 0.

Figure 4.1(a)



Linear shallow-water response, $|C_0|$ versus period, for the RPP null, mode number 0.
 Figure 4.1 (i)
 Linear shallow-water response, $|C_0|$ versus period, for the RPP null, mode number 0.

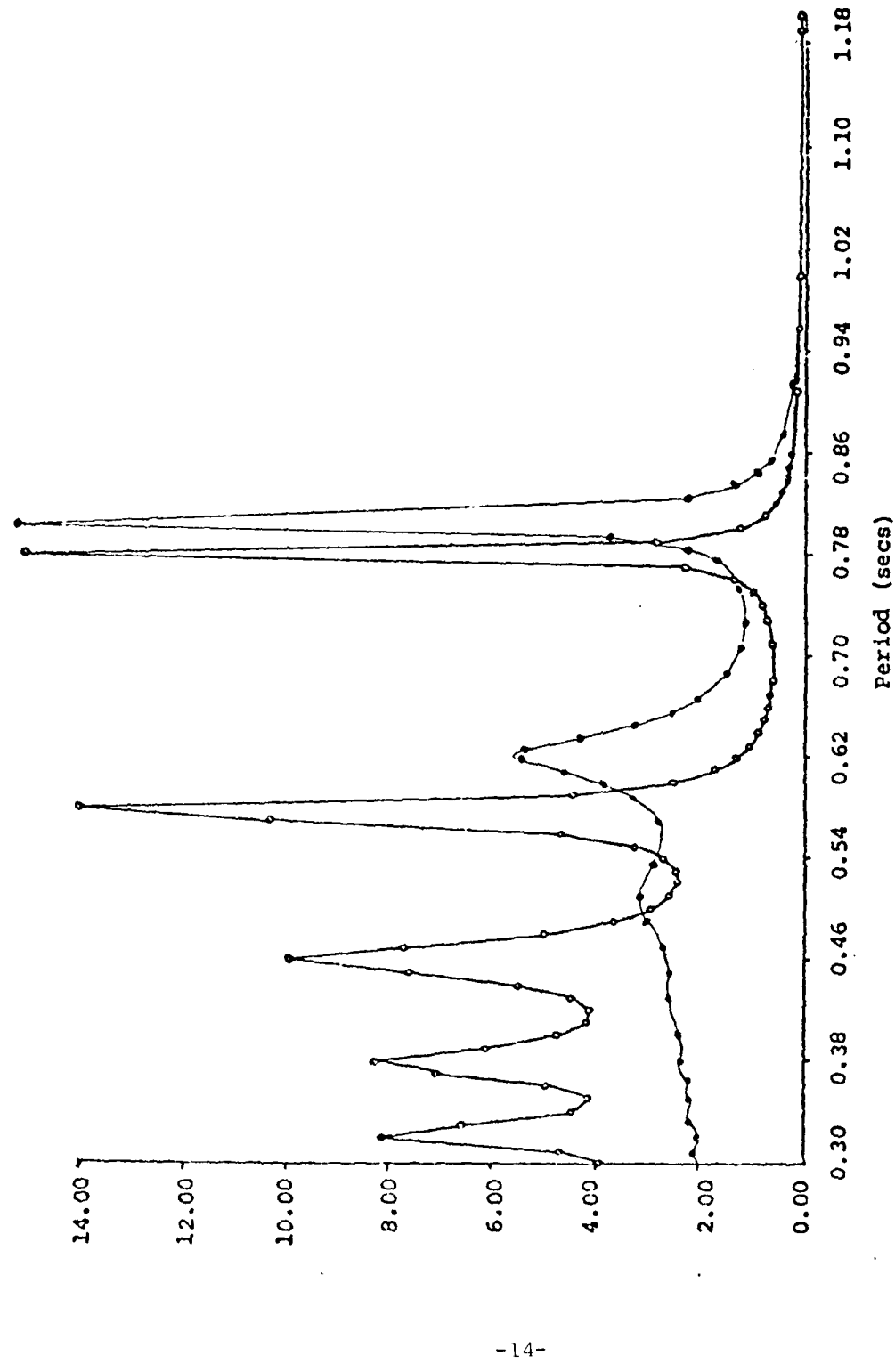


Figure 4.2

— Linear shallow-water response, $|C_6|$ versus period, for the BPP sill, mode number 6.

— Linear response $|C_6|$ versus period with no decaying modes, for the BPP sill.

$$E_2 = \left[\frac{\sum_{i=1}^7 \sum_{j=1}^{19} w_{ij} [|\eta_E(r_i, \theta_j)| - |\eta_T(r_i, \theta_j)|]^2 r_i}{\sum_{i=1}^7 \sum_{j=1}^{19} w'_{ij} |\eta_E(r_i, \theta_j)|^2 r_i} \right]^{1/2} \quad (4.1)$$

and

$$E_m = \frac{\max_{i,j} [|\eta_E(r_i, \theta_j)| - |\eta_T(r_i, \theta_j)|]}{\max_{i,j} |\eta_E(r_i, \theta_j)|} \quad (4.2)$$

The coefficients w_{ij} and w'_{ij} represent the weights determined by Simpson's rule for integration over θ ($0 < \theta < \pi$) and $r(r_1 < r < r_7)$, together with additional terms from the integration over $0 < r < r_1$ and $r_7 < r < 1$. For example, the square of the numerator of E_2 is

$$\begin{aligned} & \{s(r_1)r_1 + s(r_7)r_7 + 4(s(r_2)r_2 + s(r_4)r_4 + s(r_6)r_6) \\ & + 2(s(r_3)r_3 + s(r_5)r_5)\}/21 + (s(r_1)r_1 + s(r_7)r_7)/14 \end{aligned} \quad (4.3)$$

where, for $i = 1, \dots, 7$,

$$\begin{aligned} s(r_i) = & \pi/54 \{ 4 \sum_{j=2n, n=1, \dots, 9} (|\eta_E(r_i, \theta_j)| - |\eta_T(r_i, \theta_j)|)^2 \\ & + 2 \sum_{j=2n+1, n=1, \dots, 8} (|\eta_E(r_i, \theta_j)| - |\eta_T(r_i, \theta_j)|)^2 \\ & + (|\eta_E(r_i, \theta_1)| - |\eta_T(r_i, \theta_1)|)^2 \\ & + (|\eta_E(r_i, \theta_{19})| - |\eta_T(r_i, \theta_{19})|)^2 \} \end{aligned} \quad (4.4)$$

A consistency check of E_2 was made by using the w_{ij} and w'_{ij} according to the midpoint rule.

When only the travelling modes A_{m0} ($m = 0, \dots, 8$) were included in the computations, the improvement in E_2 over the LH theory was 8%. When the first decaying mode A_{m1} ($m = 0, \dots, 8$) was included, together with a large number of "outer" decaying modes, E_2 was further improved by 13%. With the inclusion of from 5 to 40 "sill" decaying modes, E_2 decreased by negligible amounts. These results document the importance of the decaying modes, which had previously been though negligible (Pite 1977).

The above computational results are explained as follows. The experimental conditions may be modeled by the full equation (3.8) when δ and $D\sigma^2/g$ are both small. Under these conditions, the response equation becomes approximately:

$$\begin{aligned}
 A_{m0} \{ J_m(ak/d) - k J'_m(ak/d) \left(\frac{\frac{H_m(ak/D)}{\lambda^m}}{H'_m(ak/D)} + X + Y \right) \} \\
 = F_m - F_m^* \frac{H_m(ak/D)}{H'_m(ak/D)} \quad (4.5)
 \end{aligned}$$

$$\text{where } X = \frac{-2}{\pi^3 \delta^2} \sum_{n=1}^{\infty} \frac{\sin^2 n\pi(1-\delta)}{n^3}$$

$$Y = \frac{8}{\pi^5} \sum_{p=1}^{\infty} p \sum_{n=1}^{\infty} \frac{\sin^2 n\pi(1-\delta)}{n(n^2 \delta^2 - p^2)^2} .$$

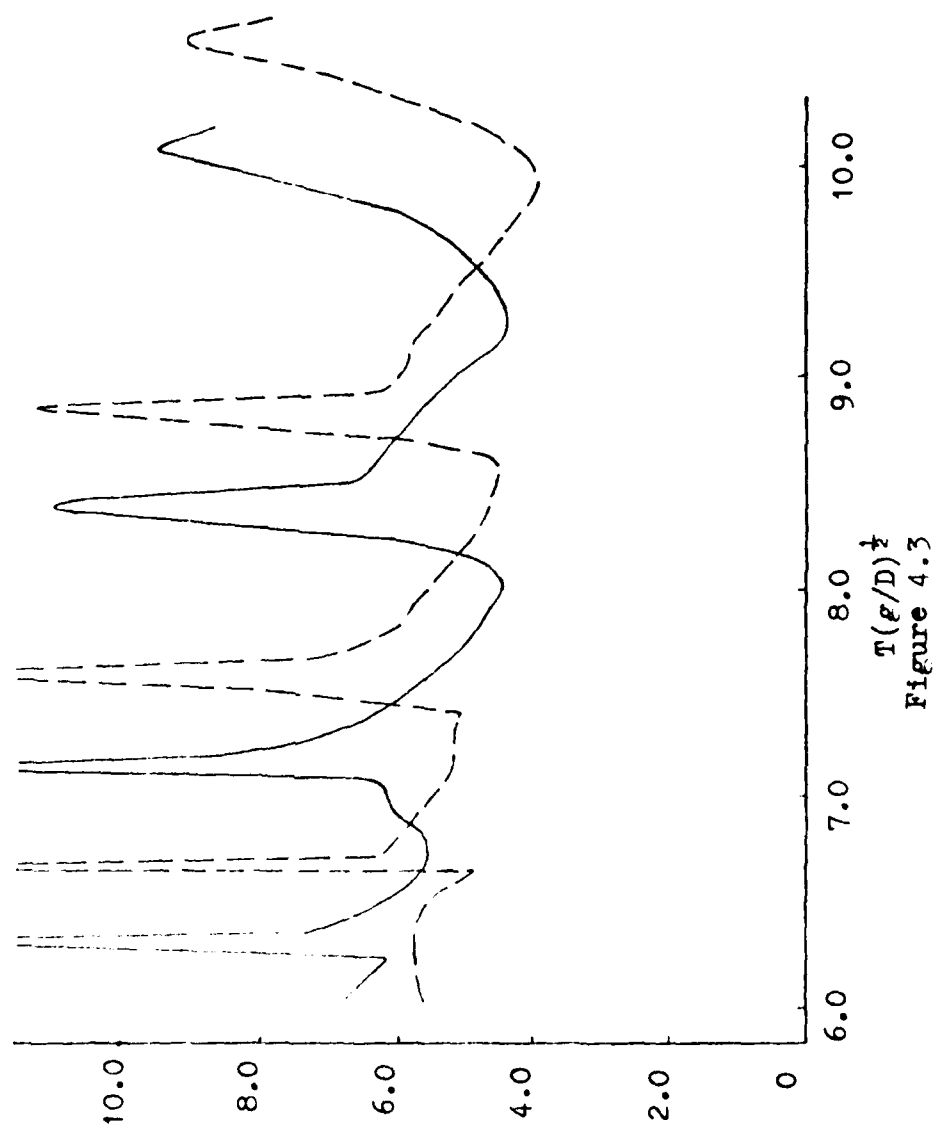
X is $O(1/\delta^2)$ and originates from the "outer" decaying modes, of which a large number must be included in the computations. Y is $O(1)$ and originates from the "sill" decaying modes. Equation (4.5) indicates that the inclusion of the "outer" decaying modes is crucial to the satisfaction of the sill-edge conditons, but that the inclusion of the "sill" decaying modes is not. This accounts for the differences in E_2 decribed in the last paragraph.

The maximum amplitudes above the sill and the amount of mechanical energy over the sill were computed using the full linear theory with 5 "sill"-decaying modes. The results, for the experimental range of forcing frequencies, are shown in figures 4.3 and 4.4 together with those of the LH theory. Compared with the peaks given by the LH theory for this range of frequencies, those of the full linear theory were shifted significantly to higher periods, with increased magnitude in the case of the 'energy' graph. The peaks of the full linear theory occur near the complex zeros of the coefficient of A_{m0} in equation (4.5). The LH theory peaks near the zeros,

$$k, \text{ of } J_m(ak/d) - \frac{k J'_m(ak/d) H_m(a\lambda/D)}{\lambda H'_m(a\lambda/D)} = 0 \text{ where } k^2 = d\sigma^2/q = \delta\lambda^2. \text{ This}$$

indicates that the shifts arise through the terms $X + Y$ which is $O(1/\delta^2)$ for small δ . The LH theory is therefore useful here only when $k/\delta^2 \ll 1$. If ak/d is too small, however, there is no resonance in the system. This indicates that the linear shallow-water theory is useful if $d\sigma^2/q$ and k/δ^2 are both small and ak/d is not small.

It appears, therefore, that a shallow-water theory is not necessarily a good approximation to the full linear theory even though the boundary conditions seem to indicate it. The reason lies in the extreme sensitivity of the matrix equation arising from (3.8) (and hence the response) to what might be presumed to be small perturbations. For example, the terms arising from the decaying modes might at first guess be thought to be unimportant, indeed, their relative excitations A_{mp}/A_{m0} for $p = 1, 2, \dots$ $m = 0, 1, \dots$ can be shown to be small. Also, the wave numbers k and λ , when evaluated by the full linear dispersion relations, differed only slightly from their shallow-water values. Their small differences, however, caused noticeable effects on



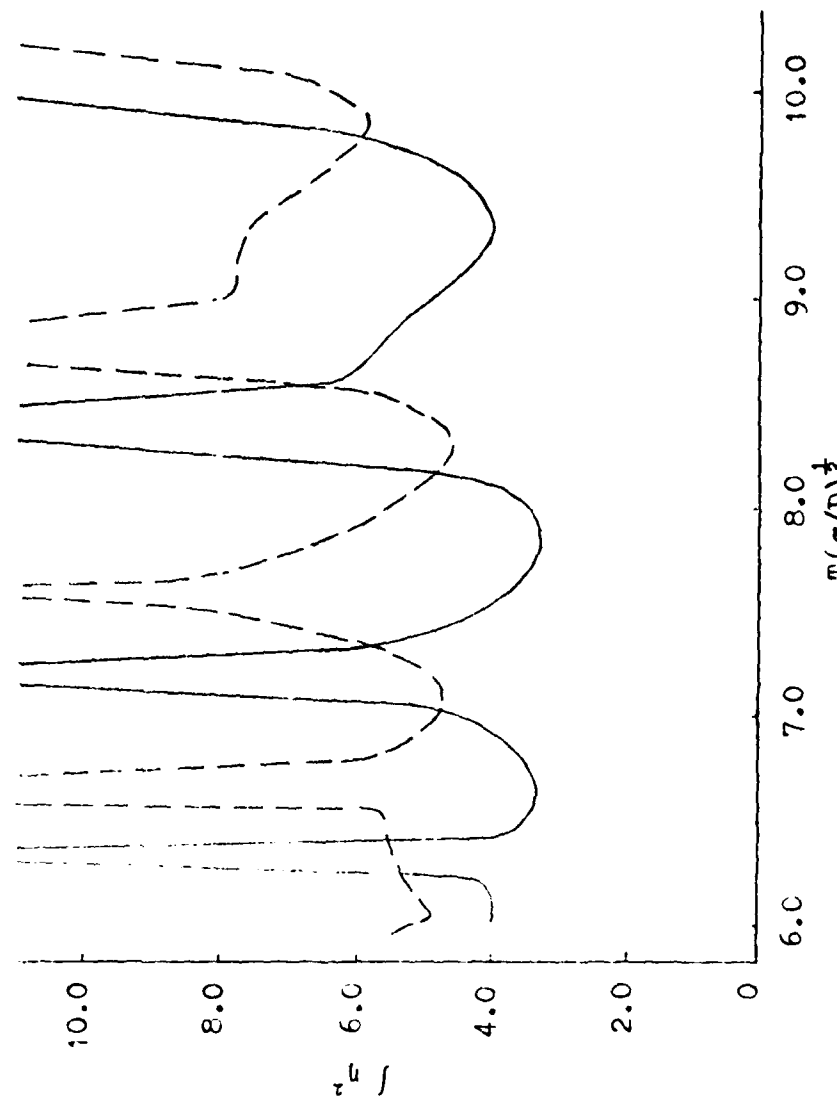


Figure 4.4
 Full linear theory
 The LH shallow-water theory

(3.8) through the Bessel functions, especially at forcing frequencies at which the resulting matrix equation was nearly singular, and these are just the frequencies of peak response. The standard, diagnostic checks on dispersion relation and modal amplitudes do turn out to mislead.

An implication of this result is that shallow-water theory should be used only with great care in interpreting experimental results concerning motions that in theory exhibit sharp changes in the response for small changes in the forcing. Another, is that great care may need to be taken with the numerical work at such frequencies.

§5. Application to oceanographic scales

LH (1967) has calculated the response $|A_n|$, where

$$\eta = \sum_{-\infty}^{\infty} e^{i(n\theta - \sigma t)} A_n J_n(k_1 r^*), \quad k_1 = \sigma/(gd)^{1/2}, \quad \text{for a selection of frequencies.}$$

The corresponding response using the full linear theory is $|C_{m0}|/\epsilon_m$, where

$$\eta = e^{-i\sigma t} \sum_{m=0}^{\infty} \cos m\theta [C_{m0} J_m(akr/d) + \sum_{n=1}^{\infty} C_{mn} \frac{I_m(ak_n r/d)}{I_m(ak_n/d)}] + *, \quad C_{m0} =$$

$$A_{m0} (id\sigma^2/g) \cosh k, \quad m = 0, 1, \dots \quad \text{and} \quad C_{mn} = A_{mn} (id\sigma^2/g) \cos k_n, \quad m = 0, 1, \dots,$$

$n = 1, 2, \dots$. The results for the frequencies and depth-ratios, δ ,

considered by LH are listed in Table 5. For $\delta = 9/16$, there were not very large differences between the predictions of the two theories. At $\delta = 1/16$, however, the LH theory predicted very large responses, especially at larger values of m . The matrix equation was then sensitive to approximations inherent in shallow-water theory, mentioned toward the end of §4, and the two theories produced very different results.

It is of interest to delineate the parameter ranges for which the shallow-water theory may be useful. This theory is based on the smallness of the parameter $D\sigma^2/g$ and the practical range for which the theory appears to be useful is limited to values of this parameter rather less than 0.1 (Table 4.1, Silvester 1974). On the other hand, the dimensionless frequencies $a\sigma/(gd)^{1/2}$ at which resonance occurs lie close to the zeros of $J_m(z)$; the smallest zeros of $J_m(z)$ increase as m increases and for m greater than 6, the first zeros are greater than 10. Since the shallow-water parameter is related to $a\sigma/(gd)^{1/2}$ by $D\sigma^2/g = (a\sigma/(gd)^{1/2})^2 (d/a)^2/\delta$, the LH theory is likely to be useful for an appropriate combination of (i) d/a small, (ii) δ not too small, and (iii) m not too large. The large, narrow, 'resonant'

Comparison of full linear theory with Longuet-Higgins' response
 $|\lambda_n|$ (1967) in the surface elevation

Mode no.	Dimensionless frequency $\frac{ag}{\sqrt{gd}}$	Longuet-Higgins $ \lambda_n $	Full linear theory's coeff. of travelling mode
2	4.921 8.219	16.23 8.057	11.88 7.267
4	7.447 10.798 14.027	91.37 18.90 8.593	2.145 5.756 6.233
6	{ 9.821 13.408 16.723 19.922 23.235	581.1 85.81 24.21 10.42 7.122	0.2798 1.176 2.840 4.331 4.196
6	12.121 15.890 19.352 22.662 25.869 29.083 32.480	3895 437.8 98.12 31.76 13.55 7.954 6.512	0.0757 0.2235 0.7472 1.714 2.797 3.269 2.769
2	4.796	2.871	2.775
3	5.632	3.269	2.921
4	6.799	3.546	3.526
5	8.021	4.447	4.482
6	{ 9.240 12.832	5.841 3.738	5.644 2.516
8	{ 11.630 15.025	10.83 3.018	5.351 3.026
5	6.8903	0.978	1.357
6	8.124	1.158	1.447
7	9.308	1.296	1.531

peaks predicted by the LH theory, however, occurred for parameter ranges not satisfying these restrictions. For instance, Table 5 ($d/a = 0.008$) shows that the most spectacular peaks occurred for the larger m and smaller δ and that these peaks were not predicted by the more accurate linear theory.

§6. Weakly viscous effects

Consider a periodic flow above the sill at a frequency σ . At the solid boundary, there will be a Stokes boundary layer of thickness $(v/\sigma)^{1/2}$, where v is the kinematic viscosity of the fluid. For laboratory scales, v is assumed to be $0.01 \text{ cm}^2 \text{ sec}^{-1}$ (for water) and for the field scales, v may be the eddy viscosity, perhaps of the order of $10 \text{ cm}^2 \text{ sec}^{-1}$. In the sill geometry of BPP, $(v/\sigma)^{1/2}d = 0.05$ and for the case considered by LH, this parameter was an order of magnitude smaller. The effect of viscous dissipation at the bottom boundary outside the sill-region is expected to be small compared with that inside. In order to estimate the effect of viscosity on the total flow, it is therefore plausible to take the boundary layer into account for $r < 1$, and to neglect it for $r > 1$. Following the work of Mahony and Pritchard (1980) the boundary condition to be posed at $z = -1$, $r < 1$, $0 < \theta < 2\pi$, is found to be

$$\frac{\partial \phi}{\partial z} = -\epsilon_1 e^{i\pi/4} \frac{\partial^2 \phi}{\partial z^2} + O(\epsilon_1^3 \epsilon_2^4)$$

where $\epsilon_1 = (v/\sigma)^{1/2}d$ and $\epsilon_2 = (d/a)^2$.

Computations for the sill geometry studied by BPP showed approximately a 1% difference in E_2 (as defined by 4.1) from the inviscid case, over the entire frequency range. Thus it would appear that the effect of viscosity is not important under their conditions. The suggestion by Pite (1977), who used a quasi-empirical theory which involves a fluctuating body-force, that viscous effects were significant on his laboratory scales, does not appear to be justifiable since his values of ϵ_1 and ϵ_2 were similar to those of BPP.

Acknowledgement

The author is indebted to Professor J. J. Mahony (University of Western Australia) for suggesting this topic and for many helpful discussions. Thanks are also due to Dr. W. G. Pritchard (University of Essex) for suggestions involving §4 and for help in drafting this paper, and to Professor R. E. Meyer (University of Wisconsin-Madison) for advice on the presentation. The work for this paper was supported in part, by a Commonwealth Postgraduate Research Award, the National Science Foundation Grant No. MCS-7927062 and the U. S. Army Contract No. DAAG29-80-C-0041.

APPENDIX

$$\varepsilon_m = \begin{cases} 1 & \text{if } m = 0 \\ 2 & \text{if } m \neq 0 \end{cases}$$

$$f(k) = \int_{-1}^0 \cosh^2 k(z+1) dz$$

$$F_m = \frac{\varepsilon_m i^{-m} J_m(\frac{a\lambda}{D})}{2\lambda \sinh \lambda}$$

$$F_m^* = \frac{\varepsilon_m i^{-m} J_m'(\frac{a\lambda}{D})}{2\lambda \sinh \lambda}$$

$$g(\lambda, k) = \int_{-1}^0 \cosh \lambda(z+1) \cosh k(z+1) dz$$

$$h(\lambda) = \int_{-\frac{1}{\delta}}^0 \cosh^2 \lambda(\delta z+1) dz$$

$$H_m(\frac{a\lambda}{D}) = H_m^{(1)}(\frac{a\lambda}{D})$$

$$H_m'(\frac{a\lambda}{D}) = H_m^{(1)'}(\frac{a\lambda}{D})$$

$$\begin{aligned}
& \left\{ \begin{array}{l}
\frac{k J_m(\frac{ak}{d})}{\delta} \left[\frac{\cosh \lambda(\delta z+1)}{\lambda h(\lambda)} \frac{H_m(\frac{a\lambda}{D})}{H'_m(\frac{a\lambda}{D})} g(\lambda, k) \right. \\
\left. + \sum_{n=1}^{\infty} \frac{K_m(\frac{a\lambda_n}{D})}{K'_m(\frac{a\lambda_n}{D})} \frac{\cos \lambda_n(\delta z+1)}{\lambda_n h(i\lambda_n)} g(i\lambda_n, k) \right] \\
\text{for } p = 0 \\
\ell_{mp}(z) = \left\{ \begin{array}{l}
\frac{k_p}{\delta} \frac{I'_m(\frac{a\lambda_p}{d})}{I_m(\frac{a\lambda_p}{d})} \left[\frac{\cosh \lambda(\delta z+1)}{\lambda h(\lambda)} \frac{H_m(\frac{a\lambda}{D})}{H'_m(\frac{a\lambda}{D})} g(\lambda, ik_p) \right. \\
\left. + \sum_{n=1}^{\infty} \frac{K_m(\frac{a\lambda_n}{D})}{K'_m(\frac{a\lambda_n}{D})} \frac{\cos \lambda_n(\delta z+1)}{\lambda_n h(i\lambda_n)} g(i\lambda_n, ik_p) \right] \\
\text{for } p \neq 0
\end{array} \right.
\end{array} \right.
\end{aligned}$$

Equations (A)

For $m = 0, 1, \dots$,

$$B_{m0} = \frac{1}{H_m'(a\lambda/D)} \left\{ \frac{1}{\partial\lambda h(\lambda)} [kA_{m0} g(\lambda, k) J_m'(ak/d) \right. \\ \left. + \sum_{n=1}^{\infty} k_n A_{mn} \frac{I_m'(ak_n/d)}{I_m(ak_n/d)} g(\lambda, ik_n)] - F_n^* \right\}$$

and for $p = 1, 2, \dots$,

$$B_{mp} = \frac{K_m(a\lambda_p/D)}{K_m'(a\lambda_p/D)} \delta_{\lambda_p} h(i\lambda_p) \left\{ kA_{m0} g(i\lambda_p, k) J_m'(ak/d) \right. \\ \left. + \sum_{n=1}^{\infty} k_n A_{mn} \frac{I_m'(ak_n/d)}{I_m(ak_n/d)} g(i\lambda_p, ik_n) \right\} .$$

Equations (B)

For $m = 0, 1, \dots$

$$A_{m0} = \frac{1}{J_m(ak/d)f(k)} \{ [B_{m0}H_m(a\lambda/D) + F_m]g(\lambda, k) \\ + \sum_{n=1}^{\infty} B_{mn}g(i\lambda_n, k) \} .$$

Here $f(k)$, F_m and $g(\lambda, k)$ are defined in the appendix.

For $p = 1, 2, \dots$

$$A_{mp} = \frac{1}{f(ik_p)} \{ [B_{m0}H_m(a\lambda/D) + F_m]g(\lambda, ik_p) \\ + \sum_{n=1}^{\infty} B_{mn}g(i\lambda_n, ik_p) \} .$$

REFERENCES

Abramowitz, M. and Stegun, I. A. (eds.) 1972. Handbook of Mathematical Functions. Washington: Nat. Bur. Stand.

Barnard, B., Pritchard, W. G. and Provis, D., To appear.

Churchill, R. V. 1963. Fourier series and boundary-value problems. McGraw-Hill.

Churchill, R. V. 1972. Operational mathematics. McGraw-Hill.

Davis, A. M. and Hood, M. J. 1976. Surface waves normally incident on a submerged horizontal cylinder. SIAM J. Appl. Math. Vol. 31, No. 1, July, pp. 28.

Havelock, T. H. 1929. Forced surface-waves on water. Phil. Mag., S. 7, Vol. 8, No. 51, Oct., 569-576.

Higher Transcendental Functions. 1953 Bateman Manuscript Project. California Inst. of Technology. A. Erdélyi (ed.). McGraw-Hill.

Longuet-Higgins, M. S. 1967. On the trapping of wave energy round islands. J. Fluid Mech. Vol. 29, part 4, 781-821.

Mahony, J. J. and Pritchard, W. G. 1978. Wave reflection from beaches. Univ. of Essex, Fluid Mech. Res. Inst., Report No. 95, June. J. Fluid Mech. 101, 809.

Meyer, R. E. 1971. Resonance of unbounded water bodies. Mathematical problems in the geophysical sciences. (W. H. Reid, ed.), Lect. Appl. Math., Vol. 13, 189-227. Am. Math. Soc., Providence, Rhode Island.

Meyer, R. E. 1979. Theory of water-wave refraction. Advances in Appl. Mech., Vol. 19, 53-141.

Phillips, O. M. 1966. The dynamics of the upper ocean. Cambridge University Press.

Pite, H. D. 1977. The excitation of damped waves diffracted over a submerged circular sill. J. Fluid Mech. Vol. 82, part 4, 621-641.

Rabinowitz, P. and Davis, P. J. 1975. Methods of numerical integration. Academic Press.

Silvester, R. 1974. Coastal Engineering, 1. Elsevier Scientific Publishing Co.

Summerfield, W. C. 1969. On the trapping of wave energy by bottom topography. Horace Lamb Centre Ocean. Res., Flinders University Res. Paper No. 30.

YY/jvs

REPORT DOCUMENTATION PAGE		READ INSTRUCTIONS BEFORE COMPLETING FORM
1. REPORT NUMBER #2195	2. GOVT ACCESSION NO. <i>AD-A100 599</i>	3. RECIPIENT'S CATALOG NUMBER
4. TITLE (and Subtitle) Trapping of Water Waves Above a Round Sill	5. TYPE OF REPORT & PERIOD COVERED Summary Report - no specific reporting period	
7. AUTHOR(s) Yuriko Yamamuro	6. PERFORMING ORG. REPORT NUMBER DAAG29-80-C-0041 MCS-7927062	
9. PERFORMING ORGANIZATION NAME AND ADDRESS Mathematics Research Center, University of 610 Walnut Street Wisconsin Madison, Wisconsin 53706	10. PROGRAM ELEMENT, PROJECT, TASK AREA & WORK UNIT NUMBERS Work Unit Number 2 - Physical Mathematics	
11. CONTROLLING OFFICE NAME AND ADDRESS See Item 18 below	12. REPORT DATE March 1981	
14. MONITORING AGENCY NAME & ADDRESS (if different from Controlling Office)	13. NUMBER OF PAGES 30	
	15. SECURITY CLASS. (of this report) UNCLASSIFIED	
	15a. DECLASSIFICATION/DOWNGRADING SCHEDULE	
16. DISTRIBUTION STATEMENT (of this Report) Approved for public release; distribution unlimited.		
17. DISTRIBUTION STATEMENT (of the abstract entered in Block 20, if different from Report)		
18. SUPPLEMENTARY NOTES U. S. Army Research Office and National Science Foundation P. O. Box 12211 Washington, D.C. 20550 Research Triangle Park North Carolina 27709		
19. KEY WORDS (Continue on reverse side if necessary and identify by block number) surface gravity water waves, diffraction, trapping modes		
20. ABSTRACT (Continue on reverse side if necessary and identify by block number) The three-dimensional problem of wave-trapping above a submerged round sill was first analyzed by Longuet-Higgins (1967) on the basis of a linear shallow-water theory. The large responses predicted by the theory were, however, not well borne out by the experiments of Barnard, Pritchard and Provis (1981) and this has motivated a more detailed study of the problem. A full, linear theory for both inviscid and weakly viscous fluid, without any shallow-water assumptions, is presented here. It reveals important limitations on the use of shallow-water theory and the reasons for them. In particular, while the qualitative features		

ABSTRACT (continued)

of wave-trapping are similar to those of shallow-water theory, the nearly-resonant frequencies differ significantly, and since the resonances are narrow, the observed amplitudes at a given frequency differ greatly. The geometry is strongly indicative of long waves and the dispersion relation appears quite consistent with that, but the part of the motion at wave numbers that are not small has, despite the small amplitude, a substantial effect on the response to excitation.

